

# Entropic organization of topologically modified ring polymers in spherical confinement

Kingkini Roychoudhury<sup>[1,2]</sup>, Shreerang Pande<sup>[1]</sup>, Indrakanty S. Shashank<sup>[1]</sup>, Debarshi Mitra<sup>[1]</sup>, and Apratim Chatterji<sup>[1]\*</sup>

1. Dept. of Physics, Indian Institute of Science Education and Research, Pune, India-411008.

2. Dept. of Physics, Indian Institute of Science Education and Research, Berhampur, India-760010

(Dated: January 7, 2025)

It has been shown that under high cylindrical confinement, two ring polymers with excluded volume interactions between monomers, segregate to two halves of the cylinder to maximize their entropy. In contrast, two ring polymers remain mixed within a sphere, as there is no symmetry breaking direction [*Nat Rev Microbiol*, **8**, 600-607 (2010)]. Therefore, in order to observe emergent organization of ring polymers in a sphere, we can introduce an asymmetric topological modification to the polymer architecture by creating a small loop and a big loop within the ring polymer. We consider the bead-spring model of polymers where there are only repulsive excluded volume interactions between the monomers ensuring that the organization we observe is purely entropy-driven. We find that for a single topologically modified polymer within a sphere, the monomers of the bigger loop are statistically more probable to be found closer to the periphery. However, the situation is reversed when we have multiple such topologically modified polymers in a sphere. The monomers of the small loops are found closer to the walls of the sphere. We can increase this localization and radial organization of polymer segments by increasing the number of small loops in each ring polymer. We study how these loops interact with each other within a polymer, as well as with loops of other polymers in spherical confinement. We compare contact maps of multiple such topologically modified polymers in a sphere. Finally, we discuss the plausible relevance of our studies to eukaryotic chromosomes that are confined within a spherical nucleus.

## I. INTRODUCTION

The organization of topologically modified polymers, with multiple internal loops along chain contour, is now a growing topic of investigation in polymer physics [1–6]. This is due to the realisation that understanding the emergent properties of such polymers is relevant for the understanding of chromosome-organization and segregation within cells [7–20].

Ring-polymer dynamics has continued to be of interest to polymer physicists since the last four decades, as ring polymers do not have any free ends. Consequently, polymer relaxation by reptation is not possible in melts of ring polymers [21–29]. There has been renewed interest in the physics of ring polymers in the last two decades, when it was realized that bacterial chromosomes having cyclic topology can be modelled as ring polymers [30–33]. It is established that the segregation of daughter chromosomes in rod-shaped bacterial cells, such as the *E.coli* [34–37], relies on the entropic repulsion between different daughter chromosomes [38–44]. We have recently shown by simulation studies that if one assumes that DNA-ring-polymers adopt specific modified polymer topologies while remaining confined in a (sphero-) cylindrical cell, then the emergent organization of polymer segments along the cell long axis is quantitatively to the organization of *E.coli* chromosomes as seen *in-vivo* [1, 45, 46]. However, deciphering the mechanisms underlying the organization of chromosomes in the cells of higher-order organisms is signifi-

cantly more complex as compared to that in bacterial cells [47]. The chromosomes of eukaryotes are confined in a spherical nucleus, and moreover there are multiple chromosomes within the nucleus. Moreover, gene regulation, carried out by linker proteins, bring different (enhancer-promoter) DNA-segments in spatial proximity and thereby create loops [48, 49]. This study is one of the first steps to investigate the physical properties of ‘*specifically designed*’ topologically modified coarse grained models of polymers with loops within spherical confinement, with the expectation that the principles elucidated from this study might be useful in the future to comprehend chromosome organization within a nucleus.

In eukaryotic cells, multiple chromosomes are compacted at various length scales within a spherical nucleus of diameter  $\approx 10\mu$ . The compaction of the double-helical DNA strands to form nucleosomes is achieved by histone proteins and leads to the formation of chromatin fiber. Moreover, there are linker proteins which connect different DNA-segments which are located far apart along the chain contour. This results in the formation of loops of different sizes along the chain contour, and may also lead to compaction and organization of the chromosome at higher length scales [50–60]. The formation of loops along the chain contour leads to the observation of topologically associated domains (TADs) [61–65].

Euchromatin, which is transcriptionally more active regions of the chromosome, is less compacted than the transcriptionally less active heterochromatin. Euchromatin segments are found towards the center of the nucleus. On the other hand, the more compacted heterochromatin is found towards the peripheral regions. Moreover, the multiple chromosomal chains within the nucleus also re-

\* Correspondence email address: apratim@iiserpune.ac.in

main spatially segregated from each other and do not get mixed with each other [66–68]. We aim to explore possibilities to develop a mechanistic understanding of the emergence of some of these observations using basic principles of polymer physics, avoiding much of the complexities inherent to chromosomes inside the nucleus of a living cell. Previous studies have proposed the idea of a fractal globule hypothesis of polymers which leads to higher contact probability between monomers along the chain contour as compared to that obtained from the statistics of a random coil. But recent investigations have considered the contact probability of polymer segments along the chain contour as a consequence of a distribution of extruded loops of different sizes within the polymer [3, 69, 70]. However, we focus on if and how entropic organization of multiple polymers can be achieved by designing topological modifications within ring polymers. These topological modifications could result from DNA-extrusion or loops formed by linker proteins.

To this end, we consider a system of many ring-polymers in spherical confinement, where we systematically modify the topology of each polymer. It is to be noted that eukaryotic chromosomes are linear polymers, but now it is also established that there are multiple loops within the linear polymer. Thus, one may imagine the DNA-polymer as a polymer with free ends with multiple hierarchical loops within the chain. In this manuscript, which is an early investigation into this topic, we use a simplified model where we neglect the free ends and possibilities of hierarchical loops. We implement multiple specifically designed loops along the chain contour by introducing additional cross-links between non-neighbouring monomers on the ring-polymer contour. Moreover, we consider identical polymers in confinement, each having the length and the same topological modifications. We investigate whether our designed topological modifications can be tuned to control the extent of segregation and/or organization of polymer segments within a sphere. These segregation and organization of polymer segments is primarily driven by tuning entropic interactions rather than by energetic interactions.

In our previous studies with topologically modified polymers in cylindrical confinement, we have established that internal loops within a ring polymer entropically repel each other, i.e., the polymer segments are able to take a larger number of configurations if the loops do not overlap. Thus, the polymer is able to explore a larger number of microstates if the loops occupy different regions along the long axis. Similarly, we establish in this study, a consequence of different-sized loops is the emergence of an asymmetry between effective entropic interactions between the polymer segments. Furthermore, asymmetric interactions between multiple such polymers confined within a sphere lead to an emergent organization of the loops (and thereby the polymer segments) along the radial direction, where smaller loops have a preference to occupy outer regions of the sphere away from the cen-

ter. This is in spite of flexible polymers being considered intrinsically disordered entities. We investigate how the relative size of the loops within a polymer, as well as the number of smaller internal loops can be tuned to play a role in the emergent organisation. Thus, we aim unearth the key principles by which topological modifications of rings leads to the radial organization of loops within a spherical confinement.

We also consider cases where the topologically modified ring-polymers can cross each other. i.e. a case where chain crossing is allowed. We implement this by suitably choosing small diameter of the bead in our bead-spring model of polymers, such that excluded volume interactions between beads does not prevent chain crossing. This is relevant because DNA-polymers are able to release topological constraints due to the presence of the enzyme topoisomerase-IV, which cuts ds-DNA strands and rejoins them after chains have crossed each other. We establish that release of topological constraints do not affect the radial organization of loops. Chain crossing also allows polymers to explore concatenated configurations. On the other hand, if one starts out with concatenations of internal loops in a packed configuration (as in a tightly folded chromosome configuration during mitosis), the DNA-polymers can also release concatenations as the daughter DNA-s unpack.

Hereon, we state the plan of the paper. In the next section, we first describe the model that we work with. Thereafter, we present the Results which has two subsections, which describe monomer organization where (i) chain crossing is not allowed and we ensure that start out with unconcatenated topologically modified ring polymers (ii) chain crossing is allowed for topologically modified ring polymers. We also plot contact maps of the different polymers, just to analyze how different segments of the polymers are in contact with particular segments of neighbouring polymers. Finally, we summarize our conclusions and discuss the future relevance of this study in the Discussion section.

## II. MODEL

We use LAMMPS [71] to perform Langevin Dynamics simulations of flexible bead-spring model of polymers. In the bead-spring model, neighbouring monomers along the chain contour interact via the harmonic spring potential with energy:  $V_{spring} = \kappa(r - a)^2$ . Here,  $r$  is the distance between the adjacent monomers along the polymer contour at the particular configuration,  $\kappa$  is the spring constant, and  $a$  is the equilibrium bond length. We use  $a$  as the unit of length in our system. Thus we express all the other lengths of other quantities, e.g. the diameter of the confining sphere in units of  $a$ . We take the value of  $\kappa$  to be  $100k_B T/a^2$ , where  $k_B T = 1$  sets the unit of energy in our simulation. The mass ( $m$ ) of the monomers are set at  $m = 1$ , such that the unit of time can be calculated as  $\tau = \sqrt{ma^2/k_B T}$ . Apart from the harmonic

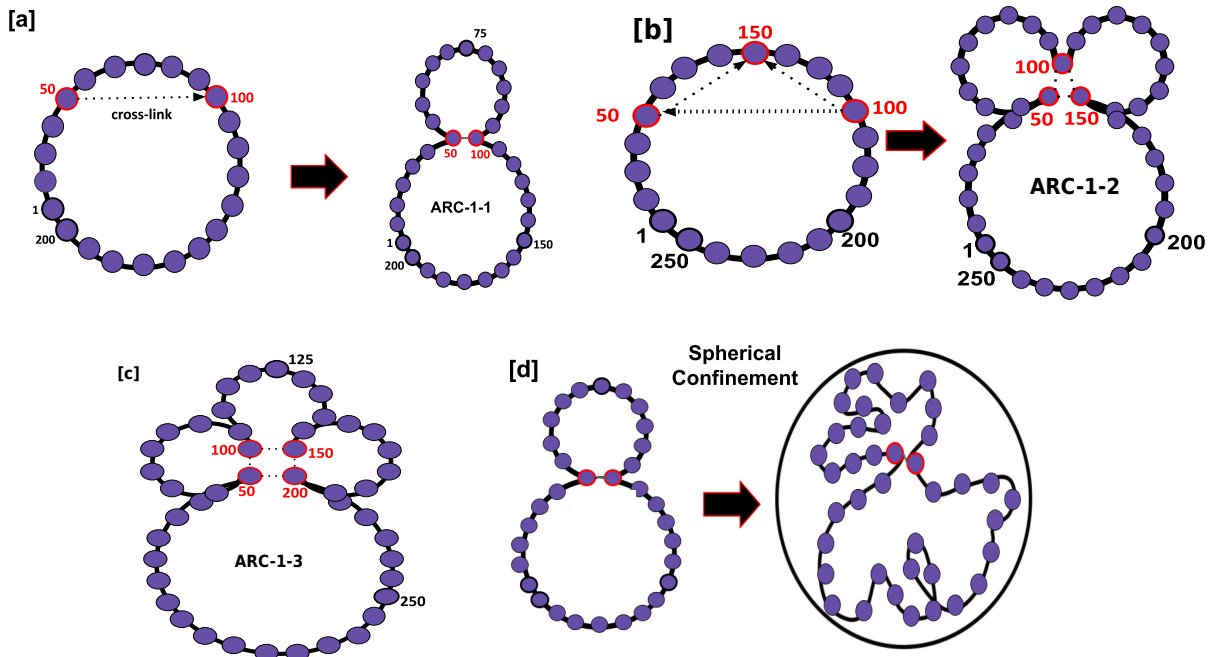


Figure 1. In this figure, we show schematics of different topologically modified ring polymers. In schematic (a), a ring polymer with 200 monomers is modified by cross-linking monomer 50 and monomer 100, i.e. we introduce a harmonic spring between the two monomers to create the topologically modified Arc-1-1 architecture. The subfigures (a), (b), and (c) schematically show bead-spring models of the Arc-1-1, Arc-1-2, and Arc-1-3, polymers, which have one, two, and three small loops, respectively, created by cross-linking the appropriate pairs of monomers. Each of the small loops have 50 monomers. Each of the architectures also have a larger loop which has 150 monomers. Hence, total number of monomers in Arc-1-1, Arc-1-2 and Arc-1-3 are 200, 250 and 300 monomers, respectively. The figure also highlights the specific monomers that have been cross-linked in order to create the loops. The light-grey lines represent the new cross-links introduced. Subfigure (d) schematically shows an Arc-1-1 polymer confined within a sphere. We maintain a volume fraction of 0.2.

spring interactions, we also add excluded volume interactions, which prevent overlap between the monomers. The excluded volume interactions follow the Weeks-Chandler Anderson (WCA) potential [72], which is given by:

$$V_{WCA} = 4\epsilon[(\sigma/r)^{12} - (\sigma/r)^6] + f_c r + \epsilon_0, \forall r < r_c. \quad (1)$$

The cut-off distance  $r_c$  of the WCA potential is given by  $2^{1/6}\sigma$ , and  $V(r) = 0$  for  $r > r_c$ . The addition of  $f_c r$  and  $\epsilon_0$  to the equation with suitable values of  $f_c$  and  $\epsilon_0$ , ensures that both the potential and the force goes smoothly to zero at the cut-off distance  $r_c$ . The diameter of the monomers is  $\sigma$ , which we take to be  $0.8a$ . This choice of  $\sigma$  also ensures that chains do not cross during the simulation. However, the choice of  $\sigma = 0.4a$ , used for *some* of our calculations implies that chains can easily cross each other, as a monomer from a different segment of the polymer can be fit in between two adjacent monomers along the chain. Note that the (phantom) spring potential just maintains the mean distance between adjacent monomers along the contour but we do not have any real material spring or chemical bonds which maintain an average distance of  $a$  between adjacent monomers along the chain contour. In our model, chain crossing is prevented as a consequence of excluded volume interactions and can

be controlled by a suitable choice of  $\sigma$ . We integrate the equations of motion using a time step  $\delta t = 0.01\tau$ .

*Polymer nomenclature:* We primarily simulate ring polymers with  $N_m$  monomers (beads) in a ring. For a ring polymer, the last monomer along the contour is connected to the first monomer by a harmonic spring interaction, with the same spring constant as mentioned above. We start with  $N_m = 200$  monomers per chain, and subsequently consider chains with larger number of monomers as we introduce topological modifications. To introduce topological modifications, we cross link specific monomers of the ring-polymer using harmonic springs of equilibrium length  $a$ . This effectively creates distinct internal loops within the ring polymer. The size of the loops, i.e. the number of monomers in the internal loops are dictated by the choice of monomers which we cross-linked. As an example, for a ring polymer with 200 monomers, we create the Arc-1-1 architecture by adding a cross-link between the 50-th and 100-th monomers, refer Fig.1a for a schematic of the architecture (topology). This effectively creates **one** big loop of 150 monomers and **one** small loop having 50 monomers. Hence, the name: Arc-1-1. Similarly, Arc-1-2 (and Arc-1-3) each have one big loop of 150 monomers and two

Architecture	$N_m = N_{sm} + N_{bg}$	$N_p$	$R_s$	$R_{actual}$
Arc-1-1	200 = 50 + 150	1	4a	4.4a
		2	5a	5.4a
		4	6.25a	6.65a
		6	7.25a	7.65a
		8	8a	8.4a
Arc-1-2	250 = 2 × 50 + 150	10	8.5a	8.9a
		1	4.25a	4.65a
		2	5.5a	5.9a
		4	6.75a	7.15a
		6	7.75a	8.15a
Arc-1-3	300 = 3 × 50 + 150	8	8.5a	8.9a
		10	9.25a	9.65a
		1	4.5a	4.9a
		2	5.75a	6.15a
		4	7.25a	7.65a
		6	8.25a	8.65a
		8	9a	9.4a
		10	9.75a	10.15a

Table I. The table lists (a) the different architectures, (b) total number of monomers  $N_m$  in each polymer (c) the number of monomers in the bigger (smaller) loops  $N_{bg}$  ( $N_{sm}$ ), (d) the number of total polymer chains in the sphere  $N_p$ , (e) the effective ( $R_s$ ) and actual radii ( $R_{actual}$ ) of the confining sphere so that volume fraction is equal to 0.2 with  $\sigma = 0.8a$ . At the end of this manuscript, we also use  $\sigma = 0.4a$  to allow chain crossing, keeping the above numbers unchanged.

(and three) small loops, respectively. Each of the small loops have 50 monomers, unless specified otherwise. Refer Fig.1(b,c) for schematics of the corresponding architecture. We choose the large loop in each polymer to have 150 monomers. Thus, when we need to be more specific about the number of monomers in each loop, we label the the polymers as Arc-1-1[150-50], Arc-1-2[150-50] and Arc-1-3[150-50] such that we can calculate the total number of monomers in the polymers as  $N_m = 200, 250, 300$ , respectively. Later we also consider Arc-1-3 polymers with 150 monomers in big loops and 25 monomers in the small loop. Thus an Arc-1-3[150-25] will have 225 monomers in the polymer.

*Radius of confining sphere:* We equilibrate  $N_p$  number of polymers in a confining sphere to study the radial organization of loops and positional distribution of monomers which are part of different internal loops of the ring polymer. The choice of the number of polymers with different topological modifications and the corresponding radius of the confining spheres has been listed in Table I.

The effective radius of the confining sphere ( $R_s$ ) is calculated in order to keep the monomer volume fraction to be equal to 0.2 with  $\sigma = 0.8a$  with  $N_p$  polymers, refer Fig.1d. Chromosomes in living cells have been reported to have volume fractions close to this value, and this inspires our choice of volume fraction. In our modelling, we ensure that the centres of the monomers to be able

to access distances of  $R_s$  from the center of the sphere, i.e. the monomer surface farthest from sphere center can be at  $R_{actual} = R_s + \sigma/2$  from the center sphere. This is implemented by the WCA potential between each of the monomers and the wall of the confining sphere. We then use this value as the actual radius of the sphere ( $R_{actual}$ ) in the simulations. The effective and actual sphere radii of the confining sphere used in all of our different cases have also summarised in Table I. When we use  $\sigma = 0.4a$ , we use the same values of  $R_{actual}$  as listed in Table I for  $N_p$  polymers, such that we have identical number density of monomers.

*Initialization and Equilibration:* We aim to investigate ring-polymers without concatenations between loops. We have taken special care to ensure that we initialize polymers within the sphere without concatenations. Thereafter, excluded volume interactions keep them unconcatenated during the course of the simulations. We initialize by placing the monomers of each chain along compact circular ring configuration, without the consideration of topological modifications due to cross-links or strong excluded volume interactions due to overlaps between the monomers in the initial configuration. The diameter of the ring is chosen to be less than that of the confining sphere. If there are multiple polymers in the sphere, then the monomers of each polymer are stacked in a ring configuration one over each other. The interaction energies are initially extremely high in the system because of excluded volume interactions between overlapping monomers, as well as stretched/compacted springs as we force the monomer to occupy adjacent positions along a circles. To relax this system, we first do off-lattice Metropolis Monte Carlo (MC) simulations from the initial configuration for  $10^5$  MC steps. The interaction potentials for the springs and the LJ interactions are kept the same as those to be used for Langevin simulations using LAMMPS. Simulations with  $10^5$  MC steps are enough to relax the system and bring the springs to their equilibrium lengths. We explicitly check by simulations in a much larger box that the polymers are free to diffuse away from each other and remain unconcatenated at the end of the Monte Carlo relaxation run. Thereafter, we use this configuration to create ten different initial conditions for independent runs, which are then used for the Langevin simulation production runs using LAMPPS. Each Langevin simulation production run is for  $2 \times 10^8$  iterations and we collect data only after  $10^8$  steps, as we allow equilibration in the presence of other polymers in the sphere for the first  $10^8$  iterations. We collect the position of each monomer in the system every  $10^4$  iterations (i.e. every  $100\tau$ ) to ensure statistical independence of polymer configurations (microstates), and use this data to calculate averaged statistical quantities to decipher the conclusions presented in the next section.

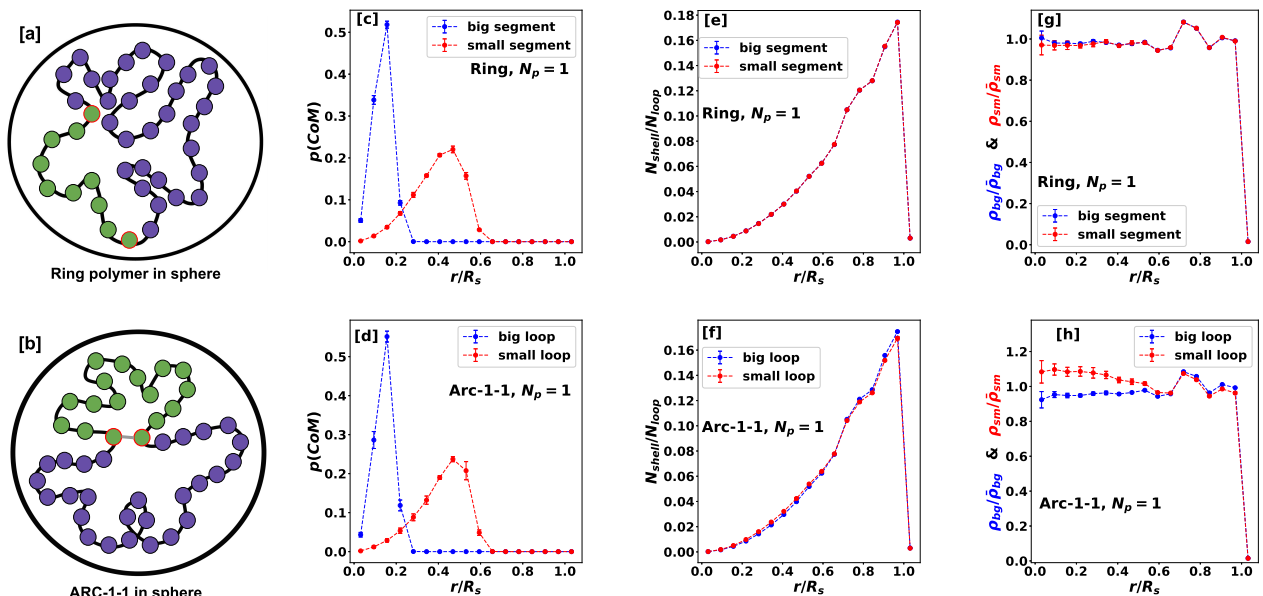


Figure 2. This set of subfigures shows the difference in organization between the two different segments of a Ring-polymer and the corresponding two segments (loops) of the Arc-1-1 polymer confined within in a sphere. Schematics (a) and (b) show a ring polymer and Arc-1-1 polymer within the sphere. Monomers between 50 to 100 correspond to the *small segment* (green circles) and is of length  $50a$  in the ring polymer. The other *big segment* (purple segments) of the ring polymer has 150 monomers. In subfigure (b), the same two monomers, i.e. the 50-th and the 100-th monomer (marked in red outline in both schematics) have been cross-linked to form two loops with 50 monomers (*small loop*) and 150 monomers (*big loop*) of the Arc-1-1 architecture. Each polymer is confined in a sphere of radius  $R = 4a$ , as mentioned in Table I. Subfigures (c) (and [d]) show the radial probability distribution of the Center of Mass (CoM) of the small and big segments (and correspondingly, small and big loops) of the ring polymer (of the Arc-1-1 polymer). The sphere is divided into concentric spherical shells of width  $\delta r = 0.25a$ , and we plot the probability of finding the CoM within each shell. Subfigures (e) and (f) show the average fraction of monomers  $N_{shell}/N_{loop}$  of a particular segment (or loop) which found in each shell, at a distance  $r$  from the center of sphere. Finally, subfigures (g) and (h) show the statistically averaged normalized monomer number densities  $\rho_{bg}/\bar{\rho}_{bg}$  and  $\rho_{sm}/\bar{\rho}_{sm}$  in each shell for the ring and the Arc-1-1 polymer, respectively. Refer text for calculation details. The error bars show the standard deviation calculated from the 10 independent runs. In each subfigure, we also mention the polymer architecture (topology) and the number of polymers  $N_p$  confined within the sphere, for the reader's quick reference.

### III. RESULTS

#### A. Organization of polymer segments in a sphere.

We now look at how the internal loops of topologically modified polymers are distributed radially in the sphere, and compare this with the distributions of segments of simple ring polymers having the same contour length and under similar confining conditions. To this end, we first compare a single Arc-1-1 architecture and a ring polymer of the same length, i.e.  $N_m = 200$  monomers. The single polymers are each confined within a sphere  $R_s = 4a$ . The choice of  $R_s$  maintains the volume fraction of monomers at  $\rho_s = 0.2$  for  $\sigma = 0.8a$ . The radius of gyration  $R_g$  of 200-monomer ring polymer in a dilute solution with good solvent without confinement is  $\approx 6.7a$  [73] (also refer Appendix) The reader may refer to Table I for the values of  $R_s$  for different cases henceforth. Figures 2(a) and (b) schematically show the ring polymer and an Arc-1-1(150-50) polymer that we compare at the start of our investigations.

To ensure equivalent comparisons such that we identify changes (if any) to the statistical distributions are solely due to the introduction of an additional CL between monomers 50 and 100 in Arc-1-1, we do the following. We choose to notionally divide the 200 monomer ring polymer into two segments with  $N_{sm} = 50$  monomers (small segment) and  $N_{bg} = 150$  monomers (big segment), respectively. This is equal to the number of monomers in the small and big loops of Arc1-1(150-50), respectively. We compare radial distributions of the center of Mass (CoM) of the two segments for the ring polymer with that of the Arc1-1 loops in Figs.2(c) and (d). We see no significant difference between the CoM distributions for the Arc1-1 and the ring polymer. Furthermore, for both cases, the distribution of the CoM of the bigger loop (segment) is closer to the center of the sphere than the CoM distribution of the smaller loop (segment).

However, the astute reader will soon realize that the CoM distribution does not reveal any information about the positional distribution of the monomers in the loops. The observation of the CoM of the big loop being close

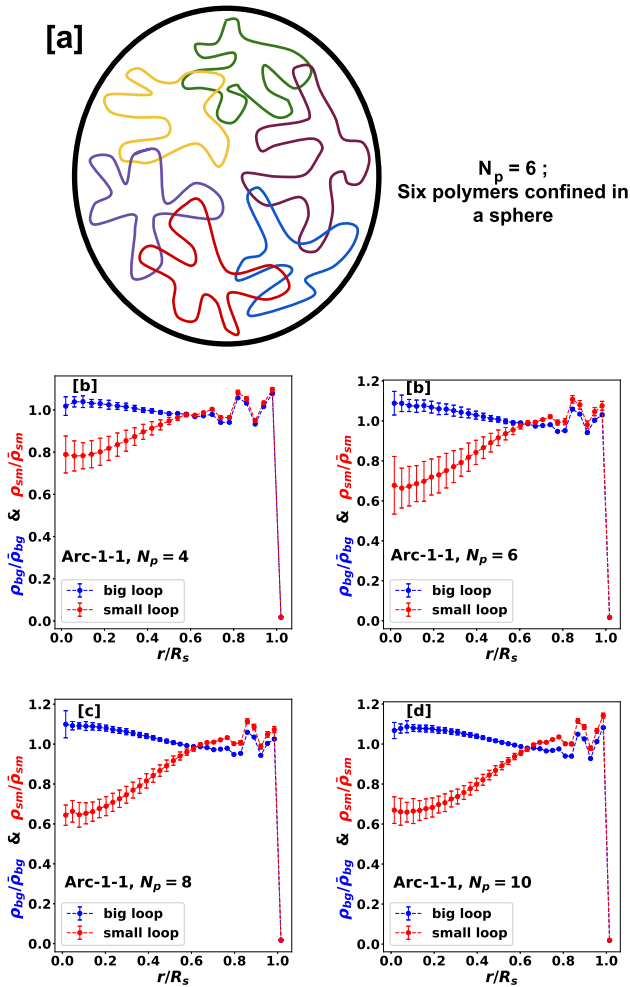


Figure 3. This figure shows the organization of the small and big loops when there are multiple Arc-1-1 polymers in the chain. The schematic in subfigure(a) shows a particular case where there are six polymers are confined in a sphere. All the polymers confined in the sphere have the same topology as we just vary the numbers of polymer chains in the sphere for different cases. Subfigures (b), (c), (d), and (e) show the normalized monomer densities, belonging to the small or big loops of the  $N_p$  Arc-1-1 polymers, as a function of the (normalized) radial distance  $r$  from the center of sphere. The number of polymers  $N_p$  within the sphere is equal to 4, 6, 8, and 10 respectively. The values of normalized monomer density of the small(or big) loop represented in the plots is the average of the values found for the small(or big) loop of each individual polymer confined in the sphere. Each subfigure has a different value of  $N_p$ , and we vary the  $R_s$  accordingly to keep volume fraction fixed. Since we are keeping the width of the shells as  $0.25a$  in every case, spheres with larger radii can contain a larger number of shells, and consequently have a larger number of data points are plotted. We use relevant monomers from all  $N_p$  polymers to calculate  $\rho_{sm}$  or  $\rho_{bg}$ .

to the sphere center may be a consequence of two different scenarios. It may mean that the monomers of the big loop are localized close to the center. However,

monomers distributed evenly close to the sphere periphery in an isotropic manner may also lead to the position of CoM being observed to be close to the center. Hence, to understand where the monomers of each segment are primarily located inside the sphere, we divide the sphere into concentric shells of different radii. We then calculate the mean of the fraction of monomers from each segment (loop)  $N_{shell}/N_{loop}$  present in each of the shells for the ring (Arc-1-1) polymer. The quantity  $N_{shell}$  is the number of monomers of each segment (loop) of the ring polymer (Arc-1-1 polymer) which are in a particular shell, and  $N_{loop}$  is the total number of monomers in the corresponding segment (loop). These plots are shown in Fig.2(e) and (f). We observe that for the ring polymer, monomers of the small and big segments are equally distributed throughout the sphere. However, by modifying the ring topology to Arc1-1, a slight difference can be seen between the distributions of the monomers of the two different loops.

As we go radially outwards, each of the spherical shells have increasingly larger volumes, and can thus accommodate more monomers. Thereby, the relevant quantity to plot is the mean number density of monomers from each segment (loop) as we move radially outwards, and moreover, normalize the mean number density of monomers in each shell by the mean density of monomers of each segment (loop) in the entire sphere. The mean number density  $\bar{\rho}_{bg}$  ( $\bar{\rho}_{sm}$ ) of the big (or small) loop in the sphere is given by  $N_{bg}/V_s$  (or  $N_{sm}/V_s$ ), where  $V_s$  is the volume of the sphere with radius  $R_s$ . The subscripts *bg* and *sm* denote the big and small segments (loops), respectively, and  $N_{bg}$  and  $N_{sm}$  are the number of monomers in big and small segments (loops) for ring (Arc-1-1) polymers. This quantity  $\rho_{sm}/\bar{\rho}_{sm}$  or  $\rho_{bg}/\bar{\rho}_{bg}$  is the normalized monomer density for the small and big segments (loops), and is plotted in Fig.2(g) and (h). This quantity measures the degree of deviation of the monomer densities of each loop/segment from the mean monomer density at different radial locations within the sphere. We first discuss the reason for observing peaks in the normalized monomer density near the wall, starting from a distance of  $\approx 0.75r/R_s$ . These peaks arise because of the presence of the wall, which creates a layer of monomers first at a distance  $\sigma/2$  from the wall surface, and further layers at distances that are multiples of  $\sigma$  from there (i.e.,  $3\sigma/2$ ,  $5\sigma/2$ , and so on) [47, 74]. At very large volume fractions(very high confinements) we would be able to observe multiple peaks. At the level of confinement that we have chosen( $\phi = 0.2$ ), we can only distinctly observe two of the peaks. These peaks disappear when we consider lower volume fraction of monomers within the sphere, as is the case when we release topological modifications of the system in a future section.

For the ring polymer, the normalised monomer densities from the big and small segments overlap as one moves out radially. This implies that the two different segments of the ring polymer have no preference to be positioned either near the center or the periphery of the

sphere. However, the big and small loops of Arc-1-1 show a clear difference between the normalized monomer densities in interior (near the center of sphere) and peripheral (near the wall of sphere) regions of the sphere. Monomers of the big loop are more probable to be found near the periphery. This is because the shells near the periphery have more volume, and the monomers can explore more configurations, i.e. higher number of microstates. Monomers of the smaller loop are relatively pushed closer to the centre of the sphere.

These plots further show that the centre of mass distribution does not give the complete picture of how monomers are localised in the sphere. The CoM distribution of the ring polymer segments are nearly identical to the distribution of CoMs of Arc1-1 loops. Since the smaller-loop and smaller-segment have equal number of monomers, the radial distribution of CoM is solely dependent on the number of monomers we consider in each segment. We further establish this observation in the following sections. Figures 2(g) and (h) firmly establish that modifying the topology by adding CLs indeed reorganises the radial distribution of probabilities of finding monomers from different segments within the sphere. Monomers of smaller loop are found preferentially near the center of sphere.

Thereafter we investigate how packing a larger number of polymer chains within the sphere changes the radial distribution of monomers. Figure 3 shows the normalised monomer density for  $N_p = 4, 6, 8,$  and  $10$  Arc1-1 polymers in a sphere of the appropriate radius. Any quantity showing the behaviour of the small (or big) loop in these cases is the average over loops from different polymers. Increasing the number of polymers shows a complete reversal in the nature of organisation that we found for a single Arc-1-1 in the sphere. In these cases, the normalised monomer density of the small loops is higher at the peripheral regions of the sphere, and the big loops are statistically found closer to the sphere centre. This means that the bigger loops remain localised closer to the centre. For multiple polymers in the sphere, the sphere diameter is proportionally larger. In this situation, the region around the sphere center has enough volume to accommodate the monomers of the bigger loops, allowing them to take up multiple configurations even as they overlap. Past studies show that rings in contact behave like soft spheres of radius approximately the size of  $R_g$  of the ring, and energy of overlap is  $\approx 5k_B T$ . This has been shown in both dilute as well as semidilute conditions [75–78]. They have found the effective interaction potentials between two ring polymers of differing sizes. It has been shown that the amplitudes of the effective interaction potential decreases as size of each ring polymer increases. Thus, the effective repulsion between each small loop is expected to be more between two smaller more compact rings than between two larger ring polymers. Thus, with multiple polymers present in the sphere, it is favourable for the big loops to overlap near the center. The small loops tend to avoid each other more and consequently,

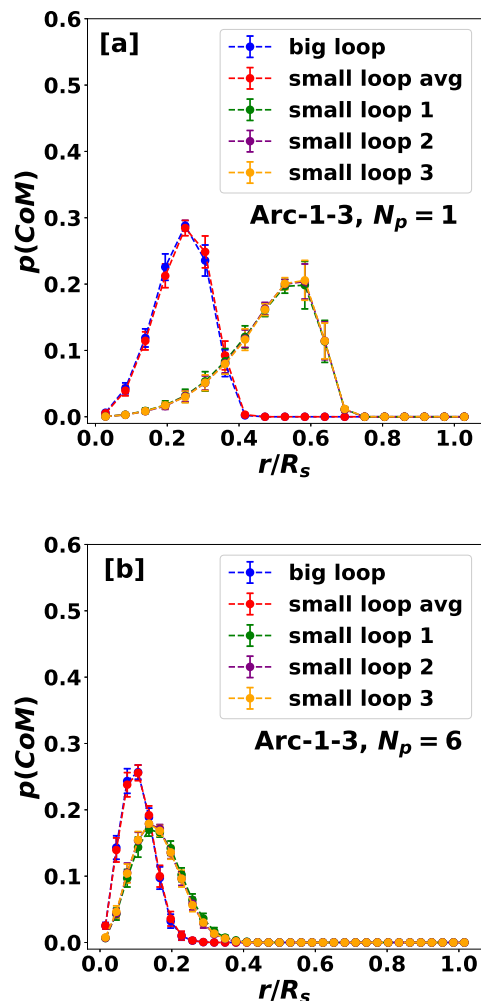


Figure 4. This figure shows the distribution of the CoM's of the different loops for Arc-1-3 polymer(s) confined in a sphere. Subfigure(a) shows the CoM distribution for Arc-1-3 polymer when  $N_p = 1$ , whereas subfigure(b) shows the distribution when there are  $N_p = 6$  Arc-1-3 polymers in the sphere. We have plotted the distribution of the CoM of the big loop, as well as the three separate CoMs of each of the three small loops of Arc-1-3. In addition, we have also averaged the CoM coordinates of the three small loops, essentially giving us the the combined CoM of the small loops. The distribution of this average CoM of the small loops is also shown above and labelled 'small loop average'. For the  $N_p = 6$  case, the plotted distributions represent the CoM distribution of big and small loops averaged over all the six different Arc-1-3 polymers.

get pushed towards the periphery. The mutual avoidance of smaller loops can also be verified later when we provide the contact maps at the end of the manuscript. The difference in the normalized monomer distribution of big loops and small loops is maximum for  $N_p = 6$ .

Next, we aim to investigate the consequences of increasing the number of smaller loops in the ring polymer architecture. We expect that this will increase the asym-

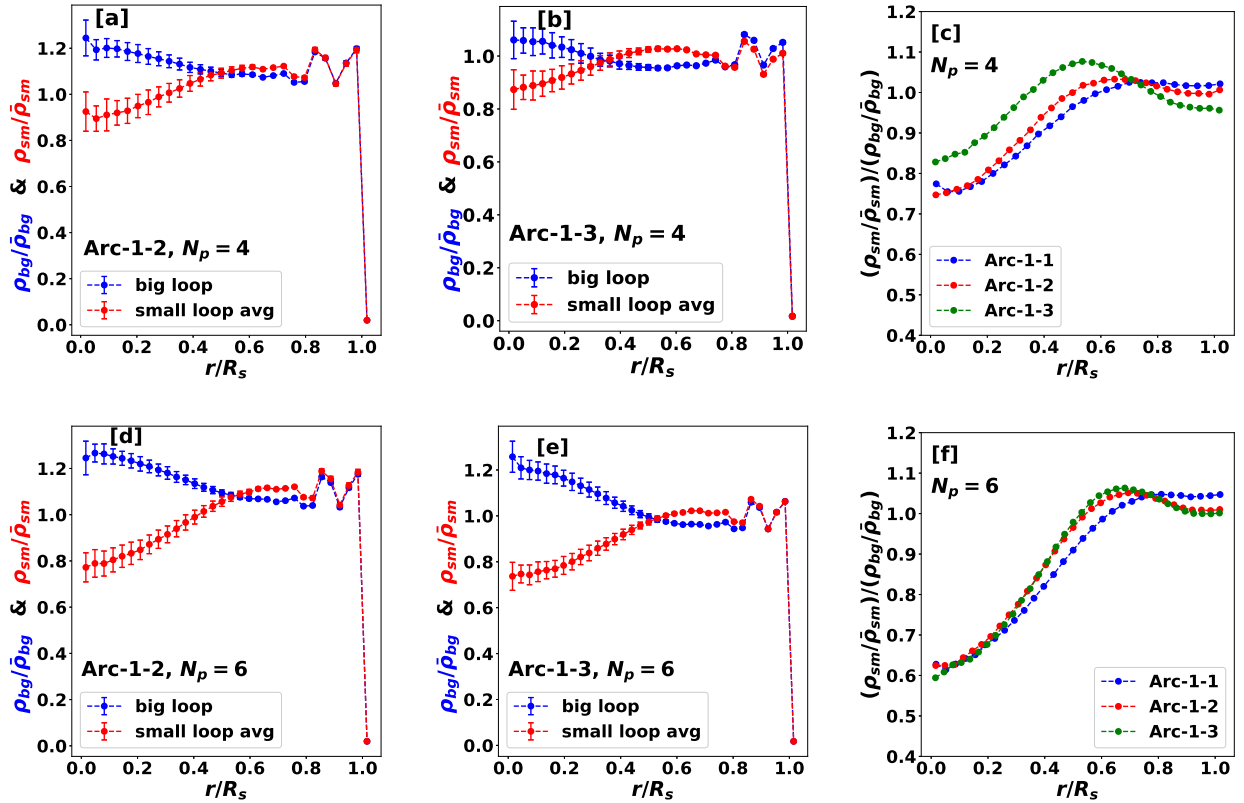


Figure 5. This figure shows the normalized monomer densities of small and big loops of Arc-1-2 and Arc-1-3 polymers for different cases of  $N_p$ . We also show the ratio of normalized monomer densities for different architectures, so that we can compare localization of smaller loops for different architectures. Subfigures (a) and (b) show the normalized monomer densities of the loops of Arc-1-2 and Arc-1-3, respectively when  $N_p = 4$ . Both Arc-1-2 and Arc-1-3 have more than one small loop, and therefore the small loop normalized monomer density plotted in the graph is the average of over monomer densities of different loops from different polymers. Subfigure (c) shows the ratio of the normalized monomer density of the small loop ( $\rho_{sm}/\bar{\rho}_{sm}$ ) to that of the big loop ( $\rho_{bg}/\bar{\rho}_{bg}$ ), for  $N_p = 4$ , in the three different architectures that we consider. Subfigures (d), (e), and (f) show the normalized densities of Arc-1-2, Arc-1-3 and the normalized density ratios for the three architectures, respectively, for the case of  $N_p = 6$ .

metry within a single polymer chain. To that end, we add two or three smaller loops, having 50 monomers in each, to a big loop of fixed length of 150 monomers. That is, we look at the properties of Arc-1-2(150-50) and Arc-1-3(150-50). In Fig.4, we begin by analyzing the CoM distribution of the loops of Arc-1-3 for two distinct cases: (i) when there is one polymer in the sphere, refer Fig.4(a), and (ii) when there are six polymers in the sphere, refer Fig.4(b). For both the cases, we see again that the CoM distributions of the individual small loops (each having 50 monomers) lie relatively away from the center of the sphere, as compared to the distribution of CoM of the big loop. In contrast, when we consider the distribution of CoM calculated using the monomers of all the three small loops, the distribution almost overlaps with that of the distribution of CoM of the big loop.

Thus, we definitively establish our previous understanding that the relative positions of the CoM of any section of the polymer is independent of the architec-

ture and solely depends on the size of the polymer segments/loops that we consider. Segments having equal number of monomers have identical CoM distributions. If we compare the CoM of two segments (or loops) of unequal lengths, the centre of mass of the segment with fewer monomers will be away from the center in the statistical sense as compared to the other. This observation is independent of whether we confine  $N_p = 1$  polymer or  $N_p > 1$  polymers within the sphere.

This also explains why the CoM distributions of the ring polymer segments and the Arc-1-1 loops were identical: the segments of ring and the loops of Arc-1-1 had an equal number of monomers. This effect occurs because the CoM of the entire polymer (or a large segment of the polymer) will always fluctuate very close to the sphere's centre. Thereby, if we take separate segments of the polymer, the CoM of the larger segment will be closer to the centre of the sphere.

In the rest of manuscript, we further look only at



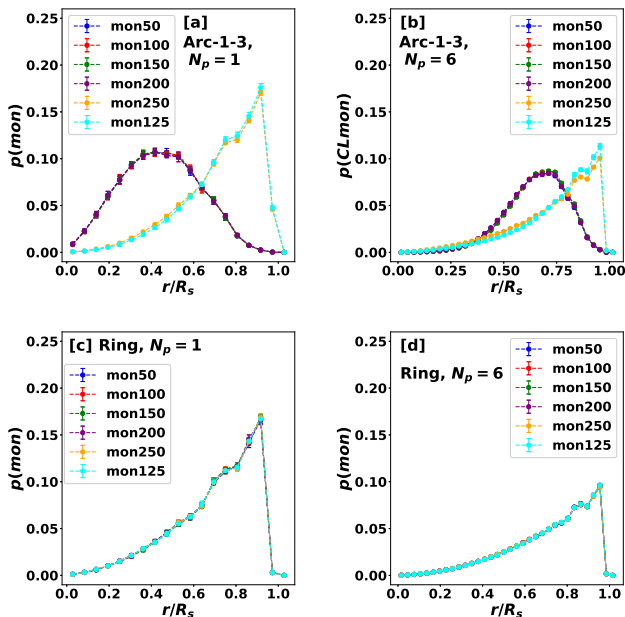


Figure 6. This figure shows the probability distributions of the position of particular monomers along the contour of the Arc-1-3(150-50) polymers. We also give data for the same monomers when we have just a ring polymer(s). Monomers with IDs 50, 100, 150, and 200 are the monomers present at the cross-links. Monomers 125 and 250 are in the middle of one of the small loops and the big loop along the contour, respectively. Subfigures (a) and (b) show the location of the cross-links in contrast to monomers in the middle of the loops, when  $N_p = 1$  and  $N_p = 6$ , respectively. Subfigures (c) and (d) show the distribution of the same tagged monomers for ring polymers of equal length. Errors bars calculated from 10 independent runs have been plotted, but can be seen for only few of the data points.

the normalized monomer densities since they show the pattern of organization of the monomers in the sphere. Figures 5 (a),(b),(d),(e) show the individual normalized monomer density plots of Arc-1-2 and Arc-1-3 for  $N_p = 4$  and  $N_p = 6$ . We see that, for both Arc-1-2 and Arc-1-3 polymers, the wall effects dominate at distances very close to the wall of the sphere, again leading to peaks in the normalized monomer densities. Due to these effects, the normalized monomer densities of both loops have nearly identical values near the wall ( $r/R_s > 0.8$ ). Although we observe that big loops have higher normalized monomer densities near the center ( $r/R_s = 0$  to  $0.2$ ) as compared to that of small loops, we should interpret this difference with care. This is because the inner shells have small radii and hence accommodate relatively fewer monomers. So small changes in the number of monomers would lead to higher fluctuations of statistical quantities at low  $r$ . Thus, we focus more on the values of normalized monomer densities  $\rho_{sm}$  and  $\rho_{bg}$  in the range:  $r/R_s = 0.2$  to  $r/R_s = 0.8$ . The small-loop monomers are found with higher probabilities at  $r/R_s > 0.5$  than the monomers of

the larger loops. In contrast, the central inner regions of sphere are primarily occupied by the monomers of the larger loops. The ratio of the normalized monomer densities from the small and big loops can go as low as  $\approx 0.6$  near  $r/R_s = 0.2$ , as can be seen in Fig.5(c) and (f). In these two subfigures, we compare data from three different architectures as it helps us evaluate the relative difference brought about in the organization by addition of smaller loops.

We can conclude from these plots that within the range:  $r/R_s = 0.5$  to  $r/R_s = 0.8$ , the ratio of the monomer densities of the small loop to the monomer densities of the big loop is  $> 1$  for all three cases. Moreover, the ratio is lowest for Arc-1-1 and takes higher values for Arc-1-2 and Arc-1-3, indicating that adding more smaller loops to the architecture increases the level of organization. Looking further radially outwards near the walls, i.e. between  $r/R_s = 0.8$  and  $r/R_s = 1$  the ratio of small loop to big loop monomer density is less than 1. This ratio is lowest for the Arc-1-3 topology. We understand this as follows: the small loops entropically repel each other and behave as soft spheres which exclude each other, as well as the wall. Moreover, the chain segments of larger loops entropically occupy the space between the soft-balls of smaller loops and the wall. For Arc-1-3, there is more space between the rosettes of smaller loops from different polymers, which is occupied by the monomers of the larger loops. The center of the sphere is also preferentially occupied by the monomers of larger loops for  $N_p \geq 4$  (refer Appendix for data with  $N_p = 2$  and  $N_p = 3$  polymers).

We also plot the distribution of radial position of monomers which constitute the cross-links (CLs), and compare it with the position of monomers which are away from the CLs. In particular, in Fig.6 we plot the radial position distribution of the specific monomers indexed 50, 100, 150 and 200 monomers, as these constitute the CLs in an Arc-1-3 architecture. We then compare the position distribution of these to the position distribution of monomers indexed as 125 and 250, which are monomers positioned away from the small loop and big loop, respectively. From the radial distributions plotted in Fig.6(a,b), we can conclude that the monomers which constitute the CLs stay away from the walls as compared to the other monomers under consideration. We present data for  $N_p = 1$  and  $N_p = 6$  cases. When  $N_p = 1$ , the CLs are closer to the sphere center. But when  $N_p = 6$ , the peak of the distribution for CLs lie in between  $r/R_s = 0.6$  and  $r/R_s = 0.8$ . In any case, cross links cannot be located too close to the periphery as it is entropically unfavourable for the three small loops which are joined at the cross-links. This is because the three smaller loops have soft sphere-like behaviour and shall surround the cross-linked monomers. Thus, monomers 125 and 250, which are away from the cross-links along the chain contour, have higher probabilities of occupying the peripheral shells. However, note that at  $r/R_s \approx 0.9$ , the value of the probability distribu-

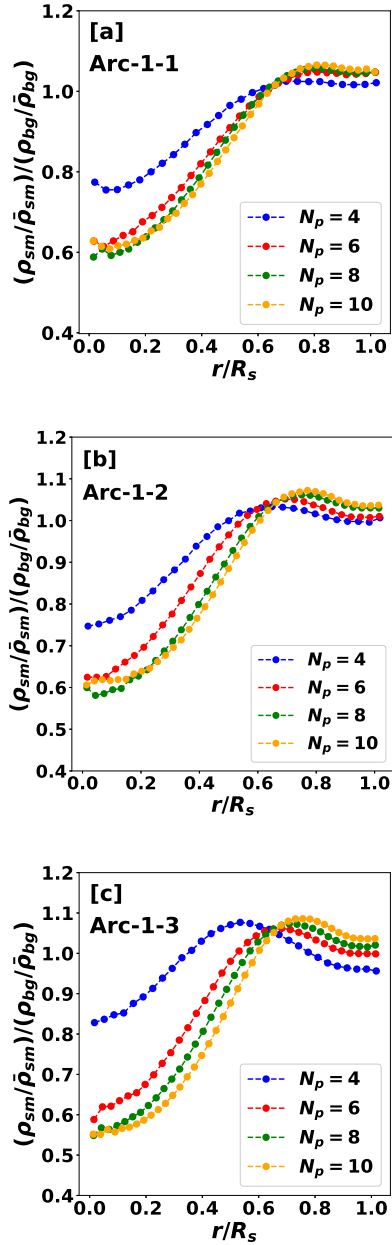


Figure 7. This figure shows the variation caused in the preferential localization of different loops in the sphere on changing the number of polymers in the sphere. The subfigures show the ratio of the normalized density of the small loop to the normalized density of the big loop for different cases of  $N_p$ . We confine different numbers of the same kind of polymer and (a), (b), and (c) shows the case when  $N_p$  number of Arc-1-1, Arc-1-2, and Arc-1-3 polymers, respectively, are confined within a sphere of appropriate radius.

tion for monomer 250 is less than the value of probability distribution of monomer 125 for both  $N_p = 1$  and  $N_p = 6$  cases. This appears counter-intuitive a priori for  $N_p = 1$  as monomers of the bigger loops are expected to be at the periphery. However, the cross-linked monomers are

close to the center and the other monomers of the smaller loops radially distribute themselves outwards from this central point. The monomers farthest away from the cross-linked monomers along the contour of the small loops thus are to be found away from the center near the peripheral regions. The data for Arc-1-3 can be compared to the control system of ring polymers with  $N_p = 1$  and  $N_p = 6$  polymers in a sphere. Here we see that all the tagged monomers have identical probability distributions for their positions, refer Fig.6(c,d).

In Figs.7 (a),(b) and (c), we establish that the localization of smaller loops to the peripheral regions of the sphere increases if we increase the number of polymers  $N_p$  of Arc-1-1 and Arc-1-2 within the sphere, but not significantly. This is shown by the comparison of the ratio of normalized monomer densities of small loops and big loops for different values of  $N_p$  for Arc-1-1, Arc-1-2, and Arc-1-3 polymers respectively. For Arc-1-3 architecture, the outlier is the  $N_p = 4$  case as the ratio becomes  $> 1$  at  $r/R_s \approx 0.4$ , but in other cases the ratio crosses 1 at  $r/R_s \approx 0.55$ . The reason for smaller loops being closer to the center is that we use a smaller confining sphere for  $N_p = 4$  as compared to systems with higher  $N_p$ . As a consequence the  $R_s \approx 7a$  is comparable to twice the radius of gyration  $R_g \approx 3a$  of the smaller loops. Thereby the data shows that the monomer density of smaller loops is closer to the center for  $N_p = 4$ .

To increase the localization of the smaller loops at the peripheral regions more significantly, we must increase the asymmetry within the polymer further. We do this by creating a new architecture of polymer with 6 small loops of 25 monomers each. The normalized monomer densities of Arc-1-3[150-25] and Arc-1-6[150-25] are plotted in Figs.8 (a) and (b). The system with 6 loops shows more significant segregation of small and large loops along the radial direction. In Fig.8 (c), we plot the ratios of the normalized monomer to compare the values of Arc-1-3[150-25] with that of our previously considered Arc-1-3[150-50]. Detailed monomer density plots of Arc-1-3[150-50] have been previously shown in Fig.5(e). We see that when number of small loops is kept the same, the radial organization is affected by the size of the small loops. By having smaller loops of 25 monomers, the level of organization increases. The data for Arc-1-6[150-25] has also been added such that we can also compare with Arc-1-3[150-50]. These two topologies have the the same number of monomer per polymer and are thereby confined in the same sized sphere.

## B. Polymers with topological constraint release.

Within the nucleus of a cell, there exists a machinery to release any topological constraints that may arise between entangled segments of the chromosomes. The enzyme Topoisomerase releases entangled configurations arising in the DNA by cutting single strands, allowing chains to cross, and then joining the strands back to-

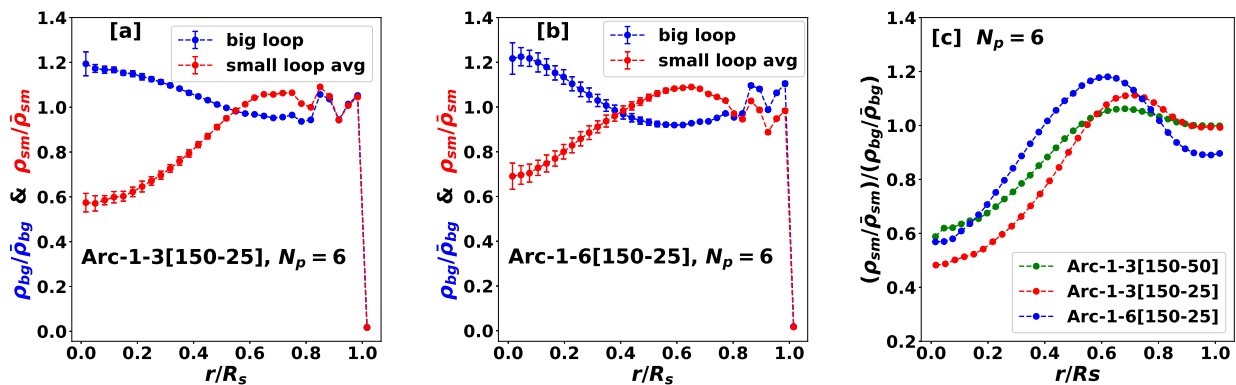


Figure 8. Subfigure(a) shows the normalized monomer densities of loops for  $N_p = 6$  polymers of the Arc-1-3[150-25] architectures with 3 small loops of 25 monomers each. This data is compared with that for Arc-1-6[150-25] in subfigure (b) to check if the number of the small loops have any effect in the localization of small loops. We also compare data of Arc-1-3[150-50] polymers with Arc-1-3[150-25] in subfigure (c) which show the ratio of normalized monomer densities for small and big loops. In subfigure (c), data for Arc-1-6[150-25] is also shown to compare with the other two topologies.

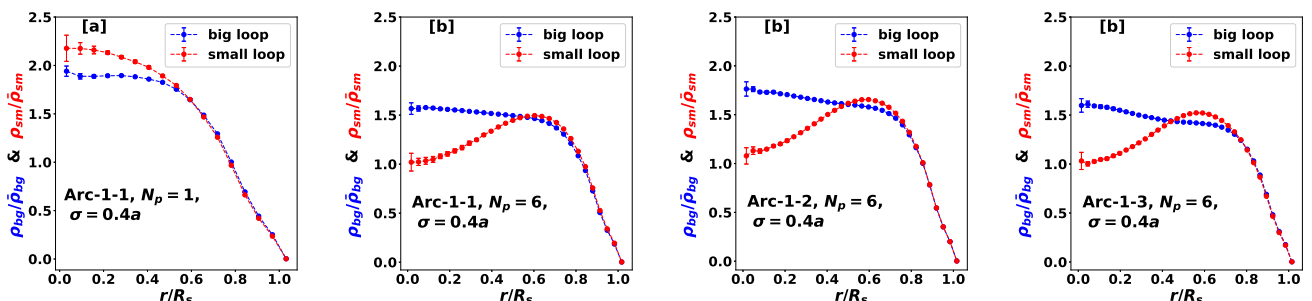


Figure 9. This figure shows the normalized monomer densities of the small and big loops of different architectures in runs where topological constraints have been released by allowing chain-crossing. Subfigure (a) shows the data for of one Arc-1-1 with  $N_p = 200$  monomers, when crossing of chains is permitted by choosing  $\sigma = 0.4a$ . The data is to be compared with Fig.2h, which considers the case where chain crossing is disallowed. Similarly, subfigures (b),(c) and (d) of this figure consider six polymers of Arc-1-1, Arc-1-2, Arc-1-3, respectively, and plot the normalized monomer densities of small and big loops with chain crossing allowed. These plots are to be compared with Figs.3c, 5d and 5e, respectively, which plot the same quantities with chain crossing disallowed. The volumes of the spheres in different cases have been kept the same as given in Table- I even when  $\sigma$  of the monomers is chosen to be  $0.4$ . This means that the volume fraction in the cases where chain crossing is allowed is less than  $0.2$ .

gether. Thus, it is pertinent to cross-check and establish that such release of topological constraints do not affect the organization of internal loops that we have found within a sphere. To that end, we also carry out polymer simulations where the mean distance between neighbouring beads in a polymer chain is maintained at  $a$ , but the diameter of the beads is chosen to be  $\sigma = 0.4a$ . This reduced bead size allows chains to cross each other as the excluded volume of each monomer is significantly reduced.

Figure 9 once again shows the radial distribution of suitably normalized monomer densities for different polymer topologies in systems where crossing of chains is allowed. In Fig.9(a), we show data when there is just one chain(Arc-1-1) within the sphere, before presenting data for multiple polymers within a sphere (Figs. 9 (b)-

(d)). The qualitative features of the positioning of loops remain unchanged, though there are quantitative differences between this data and the corresponding data where chains cannot cross. For example, there is no peak in the normalized monomer density near the periphery of the sphere, in contrast to studies with  $\sigma = 0.8a$ . Furthermore, the monomer densities gradually decay to zero near the sphere surface. This is due to the reduced excluded volume of the beads, which leads to the volume fraction in this case to be much less than  $0.2$ . We can infer that if chain crossing is allowed only intermittently such that it occurs with low probability than considered in this section, we expect loops will be positioned in the same manner as observed for the cases where chain crossing is not allowed.

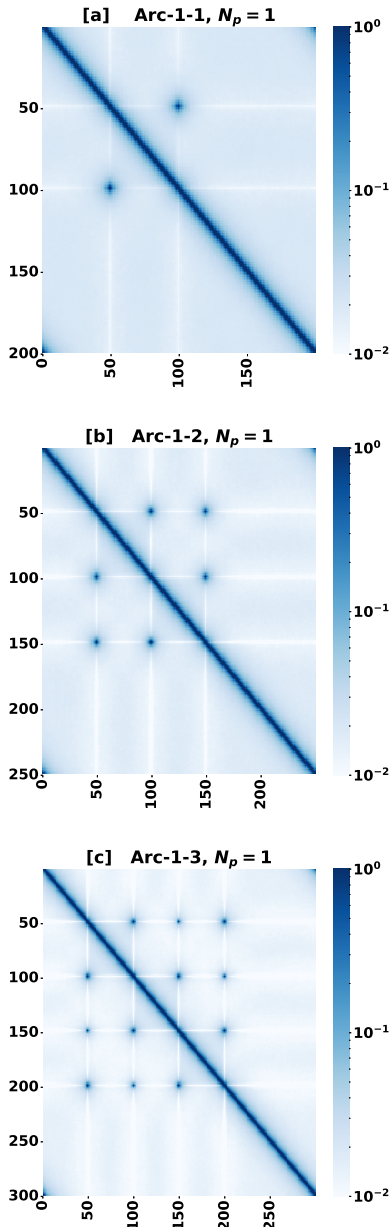


Figure 10. The above figure shows the contact maps of (a) Arc-1-1 (b) Arc-1-2, and (c) Arc-1-3 polymers, when only one polymer is confined within the sphere of radius  $R_{actual}$ , refer Table I. The color bar is in log-scale and is limited to the range  $10^{-3}$  to  $10^{-1}$ . Note that the first pair of CLs link the 51-st monomer to the 100-th monomer.

#### IV. CONTACT MAPS

To find out more information about the contact probabilities between polymer segments as we modify the polymer topology inside the sphere, we plot a contact map. If there are  $N$  total monomers in the system, a contact map of the system will be a  $N \times N$  matrix mapping the probability of close contacts of each monomer with every other

monomer. The contact map strategy is inspired by Hi-C Map experiments that reveal close contact information in chromosomes [79].

To calculate the contact map, for each micro-state we calculate the distance from of a monomer to all the other monomers in the system. If the distance between the  $i$ -th monomer and the  $j$ -th monomer is less than a selected threshold distance  $r_T$ , then we consider those two monomers to be in close contact. Thus  $i-j$  th index show the probability that two monomers are in contact with each other. The probabilities of contact is then shown as a heat-map for all pairs of monomers. Our choice of threshold distance is  $r_T = 2\sigma = 1.6a$ . Thus, we only highlight the frequencies of very close contacts, and hence there there can be pairs which rarely come in contact with each other and can have probabilities  $\ll 1$ . Thereby, the scale of the color bar is in log-scale for Fig.10; these figures shows the contact maps of a single Arc-1-1, Arc-1-2, Arc-1-3 polymers confined in a sphere.

In the figures, the main diagonal is dark in color as they show contacts of neighboring monomers along the chain contour. The off-diagonal dark spots correspond to the monomers which are cross-linked and are at a (mean) distance of  $a$ . Because of the proximity of cross-linked monomers with each other, there arises steric hindrance between the pair and other monomers of the polymer. As a consequence, we also see significantly less contact between these pair of monomers and the other monomers: these show up as horizontal and vertical white lines in the contact map. As previous studies with unconfined polymers have also shown, the monomers of a loop have a higher contact probability with each other as compared probability of contact with other monomers. These intra-loop high contacts show up as darker squares along the diagonal. Subfigures Fig.10a,b,c have one, two, three dark squares, respectively corresponding to the number of smaller loops.

Next, we would like to investigate how inter-polymer contacts get modified as a consequence of topological modifications when there are multiple polymers in the sphere. Figure 11 shows the contact maps for different topologies of polymers, ensemble averaged over 10 independent runs, where each run is  $10^6\tau$ . The same protocol was followed to obtain data shown in Fig.10. We consider six polymers of the same topology and length, confined within a sphere of the same radius. We consider four different topologies: linear polymers, ring polymers, Arc-1-3, and Arc-1-6, and for every case there are 300 monomers in a single polymer.

As expected, the diagonal is in a dark red color corresponding to very high contact probability in all the subfigures of Fig.11. In figure 11a, the relatively uniform color in the off-diagonal squares of the contact maps of the linear polymers shows that they are mixed. Differences if any, cannot be identified especially since the color bar is on logarithmic scale. The squares on the diagonal are slightly lighter-blue in colour. This means that monomers from the same polymer have a higher proba-

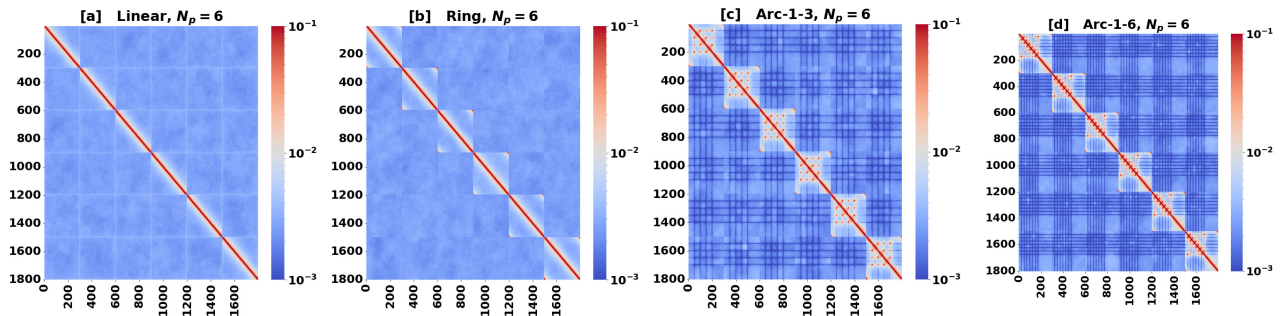


Figure 11. In this figure, the subfigures (a), (b), (c), and (d) respectively show the contact maps of linear polymers, ring polymers, Arc-1-3[150-50], and Arc-1-6[150-25] polymers confined in the sphere. Each case has  $N_p = 6$  polymers in the sphere. The Arc-1-3 and Arc-1-6 polymers show distinct polymer demixing, whereas the linear and ring polymers are more mixed. The color bar is in log-scale, and has been set to  $10^{-3}$  to  $10^{-5}$ . The color scale has been chosen such that red represents high contact(warm), blue represents low contact(cool), and white represents intermediate contact.

bility to be in contact with each other as compared to that of monomers from other polymers. The free ends of the linear polymers shown up as horizontal and vertical white lines in the contact map. In ring polymers, shown in Fig.11(b), diagonal squares are lighter, and show more self-contact within ring polymers than in linear polymers. The off-diagonal squares are almost of the same shade. In Fig.11(c), showing data for Arc-1-3, squares showing inter-polymer contact are deeper blue than squares showing intra-polymer contact. However, there is some non-uniformity that appears in the off-diagonal squares as well indicating that not all polymers(or loops of each polymer) are equally overlapped. In Arc-1-6(Fig.11(d)), the difference in color in the off-diagonal squares becomes more distinguishable. Moreover, we can distinguish that big loop-big loop contacts are more probable than small loop-small loop contact, further supporting our assumption that topology radially organizes big loops at the centre while small loops are pushed towards the periphery. Thus, on adding loops to the architectures, the polymers confined in the sphere are going from a mixed state to a relatively more segregated, or demixed state. Further systematic studies of the demixing of polymers with loops are currently underway and will be reported in a future publication.

## V. DISCUSSIONS

In this work, we have shown that the segments of a ring polymer can be entropically arranged (in a statistical sense) within a sphere by suitably modifying the internal topology. Topological modifications by introduction of internal loops of different sizes can be used to position the differently sized loops at different distances from the center of the confining sphere. The primary underlying mechanism of this phenomenon is that the loops of different sizes behave like soft repulsive spheres. The smaller loops are pushed to the outer peripheral shell of the sphere, and the inner volume is shared by the

monomers of the big loops, where they can share space and explore multiple configurations to maximize entropy, or equivalently minimize free energy. Internal energy contributions due to WCA interactions contribute minimally to the free energy; refer Appendix. However, when we have one or two polymers in the sphere, the free energy minimization is achieved by monomers of the big loops being preferentially positioned towards the periphery.

Manipulating the topology of polymers to modify the entropic interaction between different sections of a ring polymer is an interesting physical endeavour by itself. But our study is motivated to find a plausible, future use of these results to investigate chromosome organization within the nucleus. Eukaryotic chromosomes are linear polymers, with multiple internal loops which are formed by binding proteins for the purpose of gene regulation. The sizes of these internal loops can even vary due to the active process of extrusion in the interphase period of the cell cycle. Moreover, there can be hierarchical loops which can be formed which will depend on the number of extrusion events going on in parallel, as well as the position of the extrusion factors on the chain contour [69]. At the moment, for the sake of simplicity, we have considered the idealized situation where, firstly, we consider topologically modified ring polymers by neglecting the effects of free ends of linear polymers. Secondly, we consider the multiple modified ring polymers in our system to be identical in topology for each case study. However, even using such simplifying considerations, we have found that the process of entropy-maximization can cause the more compact segments of the polymers to be pushed more towards the periphery of the sphere. This is reminiscent of the more-compacted heterochromatin being situated near the periphery of the nucleus. Thus, we propose that entropic interactions could be one of the aspects affecting nuclear organization in eukaryotes, and its role should be investigated further.

By comparing contact maps of different polymers, we observe that inter-polymer contact between segments of different polymers is reduced as we introduce internal

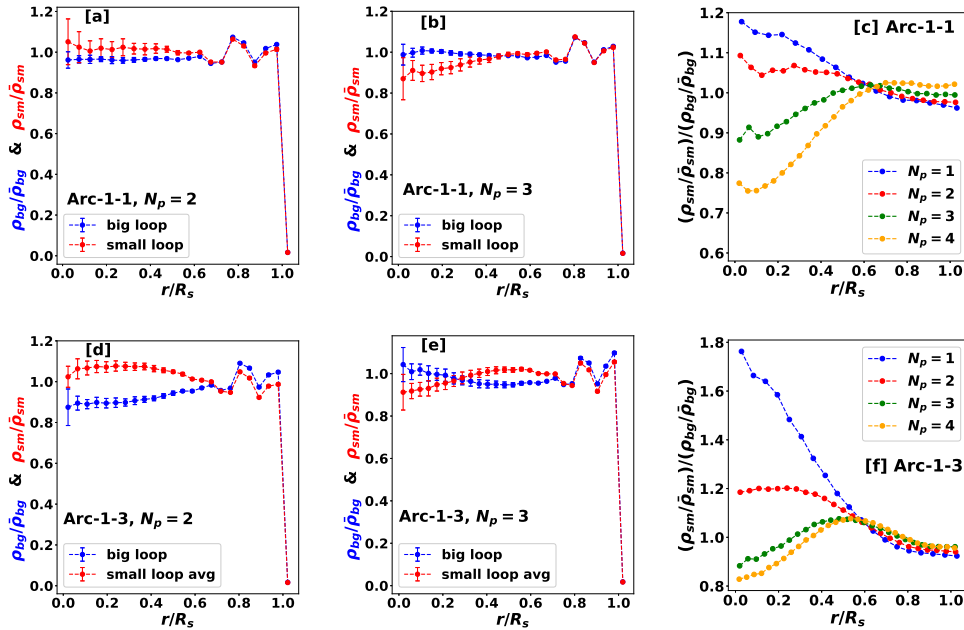


Figure 12. This figure shows normalized monomer density of the small loops and big loops when there are  $N_p = 2$  and  $N_p = 3$  polymers in the sphere for Arc-1-1 ((a)-(c)), and Arc-1-3((d)-(f)) polymers. Subfigures (c) and (f) show how the ratios of small loop monomer density to big loop monomer density changes as we go from  $N_p = 1$  to  $N_p = 4$  for Arc-1-1 and Arc-1-3 polymers respectively.

loops within the polymers. In hindsight, this observation is not unexpected, as we are introducing more internal constraints within each polymer to make it more compact, thereby possibly reducing mixing between the polymers. We are extending our current studies to systematically investigate this aspect for linear polymers with internal loops where the different polymers could have different topologies. Whether these considerations also lead to a preference for a particular polymer (chromosome) to be the neighbour of other particular polymers (other chromosomes), where the choice depends on the relative differences in topology, is an aspect which we are also investigating.

In summary, we believe that this paper and its adjoining previous study will open up further exploration of the emergent properties obtained by modifying the internal topologies of polymers. Our previously published works have already demonstrated that the bacterial cell can modify the topology of its chromosome during its cell cycle to organize itself even as replication is in progress [1, 45, 46]. We hope that the current work too, will be helpful in identifying some of the underlying mechanisms of chromosome organization in eukaryotic cells.

## VI. AUTHOR CONTRIBUTIONS

KR implemented the model, performed calculations and analysis. The research plan was designed by AC, DM and interpretation of results has extensive contribu-

tions from SP. ISS did initial calculations which started off the project. KR, DM, and AC wrote the paper.

## VII. ACKNOWLEDGEMENTS

Authors acknowledge useful discussions with Arieh Zaritsky, Conrad Woldringh, J. Horbach, and Sathish Sukumaran. AC, with DST-SERB (IN) identification No. SQUID-1973-AC-4067, acknowledges funding by DST-SERB (IN) project CRG/2021/007824, funding by Biosantexc research and mobility programs funded by ENS-France and opportunity to host Prof. Jie Xiao using funds from the Fulbright-Nehru specialist program from USIEF A.C also acknowledges discussions in meetings organized by ICTS, Bangalore, India and use of the computing facilities by PARAM-BRAHMA.

## VIII. APPENDIX:

### A. Calculation of Radius of Gyration

Estimating the radius of gyration of a single ring polymer in good solvents (in dilute solution) remains controversial [73]. In particular, one is interested to calculate the  $f$ -factor, which is the ratio of the square of the radius of gyration of a ring polymer and a linear polymer, *viz.*  $[R_g(R)/R_g(L)]^2$ . Here  $R_g(R)$  and  $R_g(L)$  is the radius of gyration of the ring polymer and the linear polymer

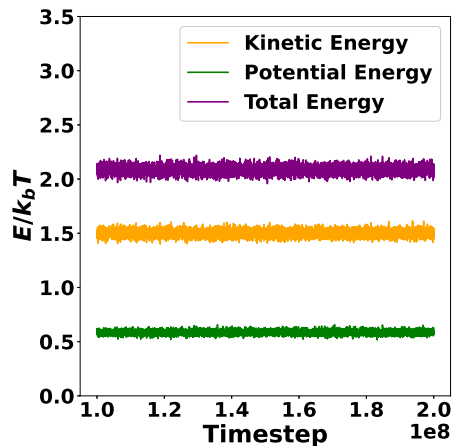


Figure 13. The figure shows the Kinetic Energy, Potential Energy, and Total Energy per monomer during a production run of  $N_p = 6$  Arc-1-3 polymers in a sphere.

with identical contour length. For a linear polymer, an estimate of the radius of gyration is

$$R_g(L) = \frac{aN^\nu}{\sqrt{(1+2\nu)(2+2\nu)}} \quad (2)$$

where  $\nu = 0.6$  is the Flory exponent for good solvents. While for a Gaussian chain, the  $f$ -factor is found to be 0.5 by analytical calculations. For real chains in good solvents, various groups have estimated different values of the  $f$ -factor, ranging from 0.516 to 0.57 [73]. We have used  $f$ -factor to be 0.55 to estimate the  $R_g(R)$  of a ring-

polymer with in good solvent with excluded volume interactions.

### B. Cases where: $N_p = 2$ and $N_p = 3$

In this section, we show the results of the simulations where we have taken either two or three polymers of the same kind within the sphere, i.e.,  $N_p = 2$  and  $N_p = 3$ . We observe that when  $N_p = 2$ , the pattern of organization is the same as that found for  $N_p = 1$ , where small loops are found preferentially towards the center, whereas for three polymers in the sphere, the small loops are located towards the periphery (Similar to what is found for higher numbers of polymers in the sphere). The same is found for both Arc-1-1(Fig. 12(a)-(c)) and Arc-1-3(Fig. 12(d)-(f)). This implies that the change in pattern of organization of loops occurs when we go from  $N_p = 2$  to  $N_p = 3$ .

### C. Change in Energy

To make sure that the organization we observe is solely due to maximization of entropy, we plotted the kinetic energy, potential energy(WCA+Spring energy), and total energy per monomer of the system across the entire production run in Fig. 13. We find that the energy of the system remains more or less constant throughout, which means that to minimize the free energy of the system, the entropy needs to be maximised which the system achieves by preferentially localizing the differently sized loops to different parts of the sphere.

- 
- [1] Debarshi Mitra, Shreerang Pande, and Apratim Chatterji. Topology-driven spatial organization of ring polymers under confinement. *Phys. Rev. E*, 106:054502, Nov 2022.
  - [2] Cristian Micheletti, Davide Marenduzzo, and Enzo Orlandini. Polymers with spatial or topological constraints: Theoretical and computational results. *Physics Reports*, 504(1):1–73, July 2011.
  - [3] Kirill E. Polovnikov, Hugo B. Brandão, Sergey Belan, Bogdan Slavov, Maxim Imakaev, and Leonid A. Mirny. Crumpled polymer with loops recapitulates key features of chromosome organization. *Physical Review X*, 13, 2023.
  - [4] Sougata Guha and Mithun K. Mitra. Multivalent binding proteins can drive collapse and reswelling of chromatin in confinement. *Soft Matter*, 19:153–163, 2023.
  - [5] N. Haddad, D. Jost, and C. Vaillant. Perspectives: using polymer modeling to understand the formation and function of nuclear compartments. *Chromosome Research*, 25(1):35–50, January 2017.
  - [6] Luca Tubiana, Gareth P. Alexander, Agnese Barbensi, Dorothy Buck, Julyan H.E. Cartwright, Mateusz Chwastyk, Marek Cieplak, Ivan Coluzza, Simon

- Čopar, David J. Craik, Marco Di Stefano, Ralf Everaers, Patrícia F.N. Faísca, Franco Ferrari, Achille Giacometti, Dimos Goundaroulis, Ellinor Haglund, Ya-Ming Hou, Nevena Ilieva, Sophie E. Jackson, Aleksandre Japaridze, Noam Kaplan, Alexander R. Klotz, Hongbin Li, Christos N. Likos, Emanuele Locatelli, Teresa López-León, Thomas Machon, Cristian Micheletti, Davide Michieletto, Antti Niemi, Wanda Niemyska, Szymon Niewieczerzal, Francesco Nitti, Enzo Orlandini, Samuela Pasquali, Agata P. Perlinska, Rudolf Podgornik, Raffaello Potestio, Nicola M. Pugno, Miha Ravnik, Renzo Ricca, Christian M. Rohwer, Angelo Rosa, Jan Smrek, Anton Souslov, Andrzej Stasiak, Danièle Steer, Joanna Sułkowska, Piotr Sułkowski, De Witt L. Summers, Carsten Svaneborg, Piotr Szymczak, Thomas Tarenzi, Rui Travasso, Peter Virnau, Dimitris Vlassopoulos, Primož Zihelr, and Slobodan Žumer. Topology in soft and biological matter. *Physics Reports*, 1075:1–137, July 2024.
- [7] Peter R. Cook and Davide Marenduzzo. Entropic organization of interphase chromosomes. *Journal of Cell Biology*, 186(6):825–834, September 2009.

- [8] Ajoy Maji, Jahir A. Ahmed, Subhankar Roy, Budhapriya Chakrabarti, and Mithun K. Mitra. A lamin-associated chromatin model for chromosome organization. *Biophysical Journal*, 118(12):3041–3050, June 2020.
- [9] Mario Nicodemi and Ana Pombo. Models of chromosome structure. *Current Opinion in Cell Biology*, 28:90–95, June 2014.
- [10] Nick Gilbert and Davide Marenduzzo. Genome organization: experiments and modeling. *Chromosome Research*, 25(1):1–4, February 2017.
- [11] Davide Michieletto, Enzo Orlandini, Matthew S. Turner, and Cristian Micheletti. Separation of geometrical and topological entanglement in confined polymers driven out of equilibrium. *ACS Macro Letters*, 9(8):1081–1085, July 2020.
- [12] Sangram Kadam, Kiran Kumari, Vinoth Manivannan, Shuvadip Dutta, Mithun K. Mitra, and Ranjith Padinhateeri. Predicting scale-dependent chromatin polymer properties from systematic coarse-graining. *Nature Communications*, 14(1), July 2023.
- [13] Shuvadip Dutta, R. Adarshkrishnan, Ranjith Padinhateeri, and Mithun K. Mitra. Protein search processes mediated by chromatin topology. December 2023.
- [14] Marco Di Stefano, Jonas Paulsen, Daniel Jost, and Marc A Marti-Renom. 4d nucleome modeling. *Current Opinion in Genetics & Development*, 67:25–32, April 2021.
- [15] Amith Z. Abdulla, Maxime M. C. Tortora, Cédric Vaillant, and Daniel Jost. Topological constraints and finite-size effects in quantitative polymer models of chromatin organization. *Macromolecules*, 56(21):8697–8709, October 2023.
- [16] Helmut Schiessel. Spatial and temporal organization of chromatin at small and large scales. *Annual Review of Condensed Matter Physics*, 14(1):193–210, March 2023.
- [17] Sophie Klempahn, Helmut Schiessel, and Ralf Blossey. Chromatin remodelers: a concise introduction for biophysicists. *Biophysical Reviews*, 16(3):357–363, June 2024.
- [18] Marc Joyeux and Ivan Junier. Requirements for dna-bridging proteins to act as topological barriers of the bacterial genome. *Biophysical Journal*, 119(6):1215–1225, September 2020.
- [19] Filippo Conforto, Yair Gutierrez Fosado, and Davide Michieletto. Fluidification of entangled polymers by loop extrusion. *Physical Review Research*, 6(3), August 2024.
- [20] Jesse R. Dixon, David U. Gorkin, and Bing Ren. Chromatin domains: The unit of chromosome organization. *Molecular Cell*, 62(5):668–680, June 2016.
- [21] Jan Smrek, Jonathan Garamella, Rae Robertson-Anderson, and Davide Michieletto. Topological tuning of dna mobility in entangled solutions of supercoiled plasmids, 2021.
- [22] Yuecheng Zhou, Kai-Wen Hsiao, Kathryn E. Regan, Dejie Kong, Gregory B. McKenna, Rae M. Robertson-Anderson, and Charles M. Schroeder. Effect of molecular architecture on ring polymer dynamics in semidilute linear polymer solutions. *Nature Communications*, 10(1), April 2019.
- [23] Thomas Vettorel, Alexander Y Grosberg, and Kurt Kremer. Statistics of polymer rings in the melt: a numerical simulation study. *Physical Biology*, 6(2):025013, July 2009.
- [24] Jonathan D. Halverson, Won Bo Lee, Gary S. Grest, Alexander Y. Grosberg, and Kurt Kremer. Molecular dynamics simulation study of nonconcatenated ring polymers in a melt. i. statics. *The Journal of Chemical Physics*, 134(20), May 2011.
- [25] Jonathan D. Halverson, Won Bo Lee, Gary S. Grest, Alexander Y. Grosberg, and Kurt Kremer. Molecular dynamics simulation study of nonconcatenated ring polymers in a melt. ii. dynamics. *The Journal of Chemical Physics*, 134(20), May 2011.
- [26] Angelo Rosa and Ralf Everaers. Conformational statistics of randomly branching double-folded ring polymers. *The European Physical Journal E*, 42(1), January 2019.
- [27] Raoul D. Schram, Angelo Rosa, and Ralf Everaers. Local loop opening in untangled ring polymer melts: a detailed “feynman test” of models for the large scale structure. *Soft Matter*, 15(11):2418–2429, 2019.
- [28] Stanard Mebwe Pachong, Iurii Chubak, Kurt Kremer, and Jan Smrek. Melts of nonconcatenated rings in spherical confinement. *The Journal of Chemical Physics*, 153(6), August 2020.
- [29] Jan Smrek and Alexander Y Grosberg. Understanding the dynamics of rings in the melt in terms of the annealed tree model. *Journal of Physics: Condensed Matter*, 27(6):064117, January 2015.
- [30] Jaehoon Shin, Andrey G. Cherstvy, and Ralf Metzler. Mixing and segregation of ring polymers: spatial confinement and molecular crowding effects. *New Journal of Physics*, 16(5):053047, May 2014.
- [31] Jaehoon Shin, Andrey G. Cherstvy, and Ralf Metzler. Polymer looping is controlled by macromolecular crowding, spatial confinement, and chain stiffness. *ACS Macro Letters*, 4(2):202–206, January 2015.
- [32] Marc Joyeux. Impact of self-association on the architectural properties of bacterial nucleoid proteins. *Biophysical Journal*, 120(2):370–378, January 2021.
- [33] Marc Joyeux. Organization of the bacterial nucleoid by dna-bridging proteins and globular crowders. *Frontiers in Microbiology*, 14, February 2023.
- [34] Anjana Badrinarayanan, Tung B.K. Le, and Michael T. Laub. Bacterial chromosome organization and segregation. *Annual Review of Cell and Developmental Biology*, 31(1):171–199, November 2015.
- [35] Conrad L. Woldringh, Flemming G. Hansen, Norbert O. E. Vischer, and Tove Atlung. Segregation of chromosome arms in growing and non-growing escherichia coli cells. *Frontiers in Microbiology*, 6, May 2015.
- [36] F J Trueba and C L Woldringh. Changes in cell diameter during the division cycle of escherichia coli. *Journal of Bacteriology*, 142(3):869–878, 1980.
- [37] Conrad L. Woldringh and Nanne Nanninga. Structural and physical aspects of bacterial chromosome segregation. *Journal of Structural Biology*, 156(2):273–283, 2006.
- [38] S. Jun and B. Mulder. Entropy-driven spatial organization of highly confined polymers: Lessons for the bacterial chromosome. *Proceedings of the National Academy of Sciences*, 103(33):12388–12393, August 2006.
- [39] Suckjoon Jun and Andrew Wright. Entropy as the driver of chromosome segregation. *Nature Reviews Microbiology*, 8(8):600–607, August 2010.
- [40] J. Pelletier, K. Halvorsen, B.-Y. Ha, R. Paparccone, S. J. Sandler, C. L. Woldringh, W. P. Wong, and S. Jun. Physical manipulation of the escherichia coli chromosome reveals its soft nature. *Proceedings of the National Academy*



- of *Sciences*, 109(40):E2649–E2656, September 2012.
- [41] Youngkyun Jung, Chanil Jeon, Juin Kim, Hawoong Jeong, Suckjoon Jun, and Bae-Yeun Ha. Ring polymers as model bacterial chromosomes: confinement, chain topology, single chain statistics, and how they interact. *Soft Matter*, 8:2095–2102, 2012.
- [42] Youngkyun Jung, Juin Kim, Suckjoon Jun, and Bae-Yeun Ha. Intrachain ordering and segregation of polymers under confinement. *Macromolecules*, 45(7):3256–3262, March 2012.
- [43] Janni Harju and Chase P. Broedersz. Physical models of bacterial chromosomes. *Molecular Microbiology*, April 2024.
- [44] Conrad L. Woldringh. Compaction and segregation of dna in escherichia coli. *Life*, 14(6):660, May 2024.
- [45] Debarshi Mitra, Shreerang Pande, and Apratim Chatterji. Polymer architecture orchestrates the segregation and spatial organization of replicating e. coli chromosomes in slow growth. *Soft Matter*, 18:5615–5631, 2022.
- [46] Shreerang Pande, Debarshi Mitra, and Apratim Chatterji. Topology-mediated organization of escherichia coli chromosome in fast-growth conditions. *Phys. Rev. E*, 110:054401, Nov 2024.
- [47] Suckjoon Jun, Axel Arnold, and Bae-Yeun Ha. Confined space and effective interactions of multiple self-avoiding chains. *Physical Review Letters*, 98(12), March 2007.
- [48] Ivan Junier, Olivier Martin, and François Képès. Spatial and topological organization of DNA chains induced by gene co-localization. *PLoS Computational Biology*, 6(2):e1000678, February 2010.
- [49] Andreas Hofmann and Dieter W. Heermann. The role of loops on the order of eukaryotes and prokaryotes. *FEBS Letters*, 589(20PartA):2958–2965, April 2015.
- [50] Anupam Mondal and Arnab Bhattacharjee. Searching target sites on dna by proteins: Role of dna dynamics under confinement. *Nucleic Acids Research*, 43(19):9176–9186, September 2015.
- [51] Tejal Agarwal, G. P. Manjunath, Farhat Habib, and Apratim Chatterji. Origin of spatial organization of DNA-polymer in bacterial chromosomes. *EPL (Europhysics Letters)*, 121(1):18004, January 2018.
- [52] Tejal Agarwal, G. P. Manjunath, Farhat Habib, and Apratim Chatterji. Bacterial chromosome organization. i. crucial role of release of topological constraints and molecular crowders. *The Journal of Chemical Physics*, 150(14):144908, April 2019.
- [53] Tejal Agarwal, G. P. Manjunath, Farhat Habib, and Apratim Chatterji. Bacterial chromosome organization. II. few special cross-links, cell confinement, and molecular crowders play the pivotal roles. *The Journal of Chemical Physics*, 150(14):144909, April 2019.
- [54] Abdul Wasim, Ankit Gupta, and Jagannath Mondal. A Hi-C data-integrated model elucidates E. coli chromosome’s multiscale organization at various replication stages. *Nucleic Acids Research*, 49(6):3077–3091, 02 2021.
- [55] Hossein Salari, Marco Di Stefano, and Daniel Jost. Spatial organization of chromosomes leads to heterogeneous chromatin motion and drives the liquid- or gel-like dynamical behavior of chromatin. *Genome research*, 32:28–43, 1 2022.
- [56] Hossein Salari, Geneviève Fourel, and Daniel Jost. Transcription regulates the spatio-temporal dynamics of genes through micro-compartmentalization. *Nature Communica-*
- tions*, 15(1), June 2024.
- [57] M. Barbieri, M. Chotalia, J. Fraser, L.-M. Lavitas, J. Dostie, A. Pombo, and M. Nicodemi. Complexity of chromatin folding is captured by the strings and binders switch model. *Proceedings of the National Academy of Sciences*, 109(40):16173–16178, September 2012.
- [58] Chris A. Brackley, James Johnson, Steven Kelly, Peter R. Cook, and Davide Marenduzzo. Simulated binding of transcription factors to active and inactive regions folds human chromosomes into loops, rosettes and topological domains. *Nucleic Acids Research*, 44(8):3503–3512, April 2016.
- [59] Andrea M. Chiariello, Carlo Annunziatella, Simona Bianco, Andrea Esposito, and Mario Nicodemi. Polymer physics of chromosome large-scale 3d organisation. *Scientific Reports*, 6(1), July 2016.
- [60] Jan Rothörl, Maarten A. Brems, Tim J. Stevens, and Peter Virnau. Reconstructing diploid 3d chromatin structures from single cell hi-c data with a polymer-based approach. *Frontiers in Bioinformatics*, 3, December 2023.
- [61] Quentin Szabo, Daniel Jost, Jia-Ming Chang, Diego I. Cattoni, Giorgio L. Papadopoulos, Boyan Bonev, Tom Sexton, Julian Gurgo, Caroline Jacquier, Marcelo Nollmann, Frédéric Bantignies, and Giacomo Cavalli. TADs are 3d structural units of higher-order chromosome organization in *Drosophila*. *Science Advances*, 4(2), February 2018.
- [62] Virginia S. Lioy, Axel Cournac, Martial Marbouty, Stéphane Duigou, Julien Mozziconacci, Olivier Espéli, Frédéric Boccard, and Romain Koszul. Multiscale structuring of the e. coli chromosome by nucleoid-associated and condensin proteins. *Cell*, 172(4):771–783.e18, February 2018.
- [63] Tung B. K. Le, Maxim V. Imakaev, Leonid A. Mirny, and Michael T. Laub. High-resolution mapping of the spatial organization of a bacterial chromosome. *Science*, 342(6159):731–734, November 2013.
- [64] Leonid A Mirny, Maxim Imakaev, and Nezar Abdenur. Two major mechanisms of chromosome organization. *Current Opinion in Cell Biology*, 58:142–152, June 2019.
- [65] Job Dekker and Leonid Mirny. The 3d genome as moderator of chromosomal communication. *Cell*, 164(6):1110–1121, March 2016.
- [66] Angelo Rosa and Ralf Everaers. Structure and dynamics of interphase chromosomes. *PLoS Computational Biology*, 4, 2008.
- [67] Angelo Rosa, Nils B. Becker, and Ralf Everaers. Looping probabilities in model interphase chromosomes. *Biophysical Journal*, 98:2410–2419, 6 2010.
- [68] Jonathan D. Halverson, Jan Smrek, Kurt Kremer, and Alexander Y. Grosberg. From a melt of rings to chromosome territories: The role of topological constraints in genome folding, 2 2014.
- [69] E. Alipour and J. F. Marko. Self-organization of domain structures by dna-loop-extruding enzymes. *Nucleic Acids Research*, 40(22):11202–11212, October 2012.
- [70] Geoffrey Fudenberg, Maxim Imakaev, Carolyn Lu, Anton Goloborodko, Nezar Abdennur, and Leonid A. Mirny. Formation of chromosomal domains by loop extrusion. *Cell Reports*, 15(9):2038–2049, May 2016.
- [71] A. P. Thompson, H. M. Aktulga, R. Berger, D. S. Bolinteanu, W. M. Brown, P. S. Crozier, P. J. in ’t Veld, A. Kohlmeyer, S. G. Moore, T. D. Nguyen, R. Shan,

- M. J. Stevens, J. Tranchida, C. Trott, and S. J. Plimpton. LAMMPS - a flexible simulation tool for particle-based materials modeling at the atomic, meso, and continuum scales. *Comp. Phys. Comm.*, 271:108171, 2022.
- [72] M. P. Allen and D. J. Tildesley. *Computer simulation of liquids*. Oxford University Press, Oxford, second edition edition, 2017.
- [73] Aritra Santra and J. Ravi Prakash. Universality of dilute solutions of ring polymers in the thermal crossover region between theta and athermal solvents. *Journal of Rheology*, 66(4):775–792, June 2022.
- [74] J.G. Powles M. Calleja, A.N. North and G. Rickayzen. The structure of fluids confined to spherical pores: theory and simulation. *Molecular Physics*, 73(5):973–983, 1991.
- [75] Arturo Narros, Angel J. Moreno, and Christos N. Likos. Influence of topology on effective potentials: Coarse-graining ring polymers. *Soft Matter*, 6:2435–2441, 6 2010.
- [76] Marco Bernabei, Petra Bacova, Angel J. Moreno, Arturo Narros, and Christos N. Likos. Fluids of semiflexible ring polymers: effective potentials and clustering. *Soft Matter*, 9(4):1287–1300, 2013.
- [77] Arturo Narros, Christos N Likos, Angel J Moreno, and Barbara Capone. Soft matter multi-blob coarse graining for ring polymer solutions. 10:9587–9758.
- [78] Arturo Narros, Angel J. Moreno, and Christos N. Likos. Architecture-induced size asymmetry and effective interactions of ring polymers: Simulation and theory. *Macromolecules*, 46(23):9437–9445, November 2013.
- [79] Sanjay Chahar, Yousra Ben Zouari, Hossein Salari, Dominique Kobi, Manon Maroquenne, Cathie Erb, Anne M. Molitor, Audrey Mossler, Nezh Karasu, Daniel Jost, and Tom Sexton. Transcription induces context-dependent remodeling of chromatin architecture during differentiation. *PLOS Biology*, 21(12):e3002424, December 2023.